

RESEARCH ARTICLE

10.1002/2016JB013577

Special Section:

Rock Physics of the Upper Crust

Theoretical modeling insights into elastic wave attenuation mechanisms in marine sediments with pore-filling methane hydrate

H. Marín-Moreno¹ , S. K. Sahoo^{1,2}, and A. I. Best¹ ¹National Oceanography Centre, University of Southampton Waterfront Campus, Southampton, Hampshire, UK, ²National Oceanography Centre, University of Southampton, Southampton, Hampshire, UK

Key Points:

- Pore-filling hydrate in sediments enhances elastic wave attenuation at 1–1E6 Hz due to increased fluid-solid contacts and squirt flow
- Hydrate-formed pores of different aspect ratios enhance elastic wave attenuation at 1E4–1E6 Hz and fluid inclusions in hydrate at 1–1E6 Hz
- Elastic wave attenuation due to fluid inclusions in hydrate may provide signal contrasts to detect pore-filling hydrate in seismic surveys

Supporting Information:

- Supporting Information S1
- Data Set S1

Correspondence to:

H. Marín-Moreno,
hector.marin.moreno@noc.ac.uk

Citation:

Marín-Moreno, H., S. K. Sahoo, and A. I. Best (2017), Theoretical modeling insights into elastic wave attenuation mechanisms in marine sediments with pore-filling methane hydrate, *J. Geophys. Res. Solid Earth*, 122, 1835–1847, doi:10.1002/2016JB013577.

Received 21 SEP 2016

Accepted 23 FEB 2017

Accepted article online 27 FEB 2017

Published online 15 MAR 2017

Abstract The majority of presently exploitable marine methane hydrate reservoirs are likely to host hydrate in disseminated form in coarse grain sediments. For hydrate concentrations below 25–40%, disseminated or pore-filling hydrate does not increase elastic frame moduli, thus making impotent traditional seismic velocity-based methods. Here, we present a theoretical model to calculate frequency-dependent *P* and *S* wave velocity and attenuation of an effective porous medium composed of solid mineral grains, methane hydrate, methane gas, and water. The model considers elastic wave energy losses caused by local viscous flow both (i) between fluid inclusions in hydrate and pores and (ii) between different aspect ratio pores (created when hydrate grows); the inertial motion of the frame with respect to the pore fluid (Biot's type fluid flow); and gas bubble damping. The sole presence of pore-filling hydrate in the sediment reduces the available porosity and intrinsic permeability of the sediment affecting Biot's type attenuation at high frequencies. Our model shows that attenuation maxima due to fluid inclusions in hydrate are possible over the entire frequency range of interest to exploration seismology (1–10⁶ Hz), depending on the aspect ratio of the inclusions, whereas maxima due to different aspect ratio pores occur only at sonic to ultrasound frequencies (10⁴–10⁶ Hz). This frequency response imposes further constraints on possible hydrate saturations able to reproduce broadband elastic measurements of velocity and attenuation. Our results provide a physical basis for detecting the presence and amount of pore-filling hydrate in seafloor sediments using conventional seismic surveys.

1. Introduction

Methane stored in seafloor hydrate is a relatively clean fossil fuel resource that has the potential to ease the transition to renewable energy in future. Methane stored in hydrate-bearing sands presently forms the most commercially attractive hydrate reservoirs [Boswell and Collett, 2011], whether on the seafloor or in terrestrial permafrost regions. Natural hydrates hosted in sediments commonly exist in several forms: (i) disseminated hydrate grows freely in the pore space away from grain contacts and is known as pore-filling hydrate; (ii) hydrate contacting neighboring mineral grains, known as load-bearing hydrate, is common for pore-filling hydrate saturations exceeding 25–40%; and (iii) hydrate forming cement between mineral grains, known as cementing hydrate (Figure 1; Waite *et al.* [2009]). In coarse grain deposits, hydrates are prone to exhibit a disseminated pore-filling habit [Zhao *et al.*, 2015] for hydrate saturations below 40% when formed from dissolved methane [Spangenberg and Kulenkampff, 2006]. Pore-filling hydrates have been directly observed and/or inferred from geophysical surveys in fine to coarse sands in locations such as Mallik, Mackenzie Delta [Uchida *et al.*, 2000], the eastern Nankai Trough [Konno *et al.*, 2015; Priest *et al.*, 2015; Santamarina *et al.*, 2015], the Ulleung Basin, East Sea of Korea [Lee *et al.*, 2013], the Okushiri Ridge, Japan Sea [Tamaki *et al.*, 1990], Alaminos Canyon, Gulf of Mexico [Boswell *et al.*, 2009], and Mount Elbert, Alaska North Slope [Stern *et al.*, 2011; Winters *et al.*, 2011]. As such, pore-filling hydrate could account for a significant proportion of global seafloor- and permafrost-hosted methane hydrates.

While the stability field of natural hydrates is readily determined, the saturation of hydrate within it is not. Estimates come from direct sampling, well log data, or remote geophysical data [e.g., Ecker *et al.*, 1998; Ecker *et al.*, 2000; Guerin and Goldberg, 2002; Matsushima, 2006; Weitemeyer *et al.*, 2006; Westbrook *et al.*, 2008; Lee *et al.*, 2013; Goswami *et al.*, 2015; Konno *et al.*, 2015]. Good indirect estimates rely entirely in our conceptual understanding of how *P* and *S* wave velocity and attenuation [Lee, 2002; Yun *et al.*, 2005; Chand *et al.*, 2006; Priest *et al.*, 2006; Waite *et al.*, 2009; Dai *et al.*, 2012; Best *et al.*, 2013], and electrical resistivity [Spangenberg, 2001;

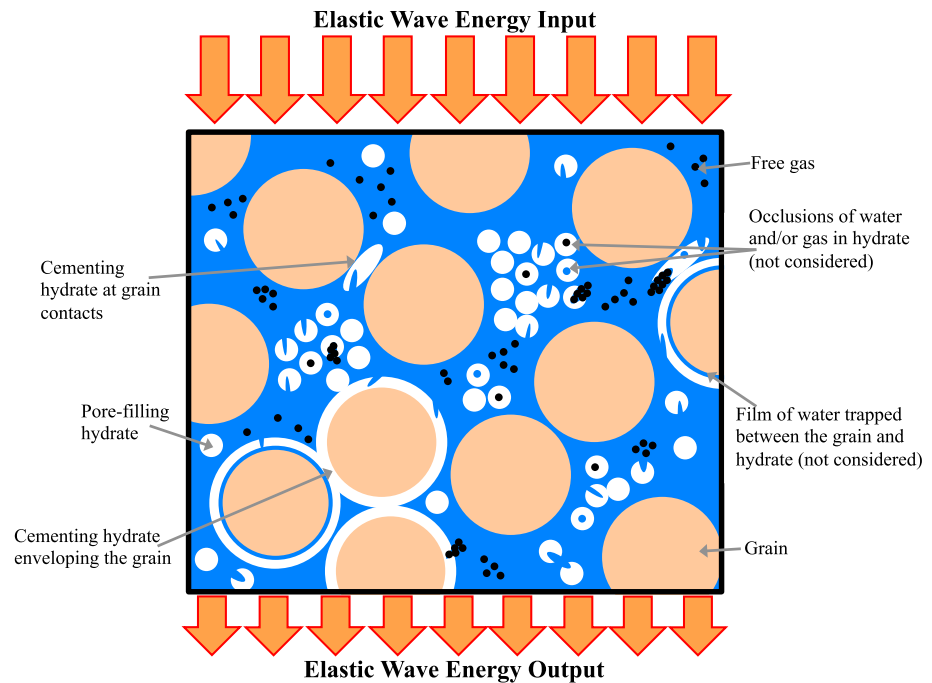


Figure 1. Idealized conceptual illustration of the microstructure of hydrate-bearing sediments (not to scale).

Spangenberg and Kulenkampff, 2006] relate to hydrate saturation and habit and in the associated effectiveness of our models. The P and S wave velocities of sediments hosting cementing hydrate, both when hydrate coats and cements grain contacts or when hydrate forms only at grain contacts, are higher than those of the sediment without hydrate because the hydrate contributes to support any pressure loading. This is reflected in an increase of the composite's bulk and shear moduli [*Ecker et al., 1998*] even for low hydrate saturations below approximately 40% [*Priest et al., 2009; Waite et al., 2009; Dai et al., 2012*]. In contrast, sediments hosting pore-filling hydrate with saturations below approximately 25–40% do not show significant changes in P and S wave velocities [*Priest et al., 2009; Waite et al., 2009; Dai et al., 2012*] because the hydrate is suspended within the water and hence only increases the bulk modulus of the effective pore fluid [*Ecker et al., 1998*]. For pore-filling hydrate saturations above 25–40%, hydrate starts bridging sediment grains, and the elastic frame moduli and associated P and S wave velocities progressively increase [*Waite et al., 2009; Dai et al., 2012*].

P and S wave attenuation may be used as an alternative indirect geophysical parameter to estimate hydrate saturation [*Guerin and Goldberg, 2002; Priest et al., 2006; Best et al., 2013*], and it is indeed an attractive alternative especially in pore-filling hydrate-bearing reservoirs where traditional P and S wave velocity methods are not effective. However, current economically exploitable hydrate-bearing sand reservoirs are likely to have hydrate saturations above 40% and thus unlikely to present, initially, a pore-filling hydrate habit. Even in this case, though, sediment shearing occurs during hydrate production [*Hyodo et al., 2013*] and when hydrate saturations start to be less than approximately 40%, it is sensible to think that pore-filling hydrate may become an important habit. Also, laboratory experiments on cementing and load-bearing hydrate show that repeated cycles of hydrate dissociation and formation tend to create a pore-filling distribution in an excess water environment [*Choi et al., 2014*]. This behavior is also likely to occur during production because of hydrate re-formation.

In situ measurements of elastic wave energy losses caused exclusively by the presence of hydrate in sediments are challenging because (i) it is difficult to isolate elastic wave energy losses within the sediment from elastic wave scattering in spatially heterogeneous media [*Huang et al., 2009*] and (ii) our understanding of the multiple energy loss mechanisms coexisting in hydrate-bearing sediments is still limited [*Priest et al., 2006; Best et al., 2013*]. Here, to overcome the above limitations, we work with attenuation differences between the hydrate-bearing sediment and the host sediment without hydrate and present a novel approach, the Hydrate-Bearing Effective Sediment (HBES) model, to integrate state-of-the-art understanding and models

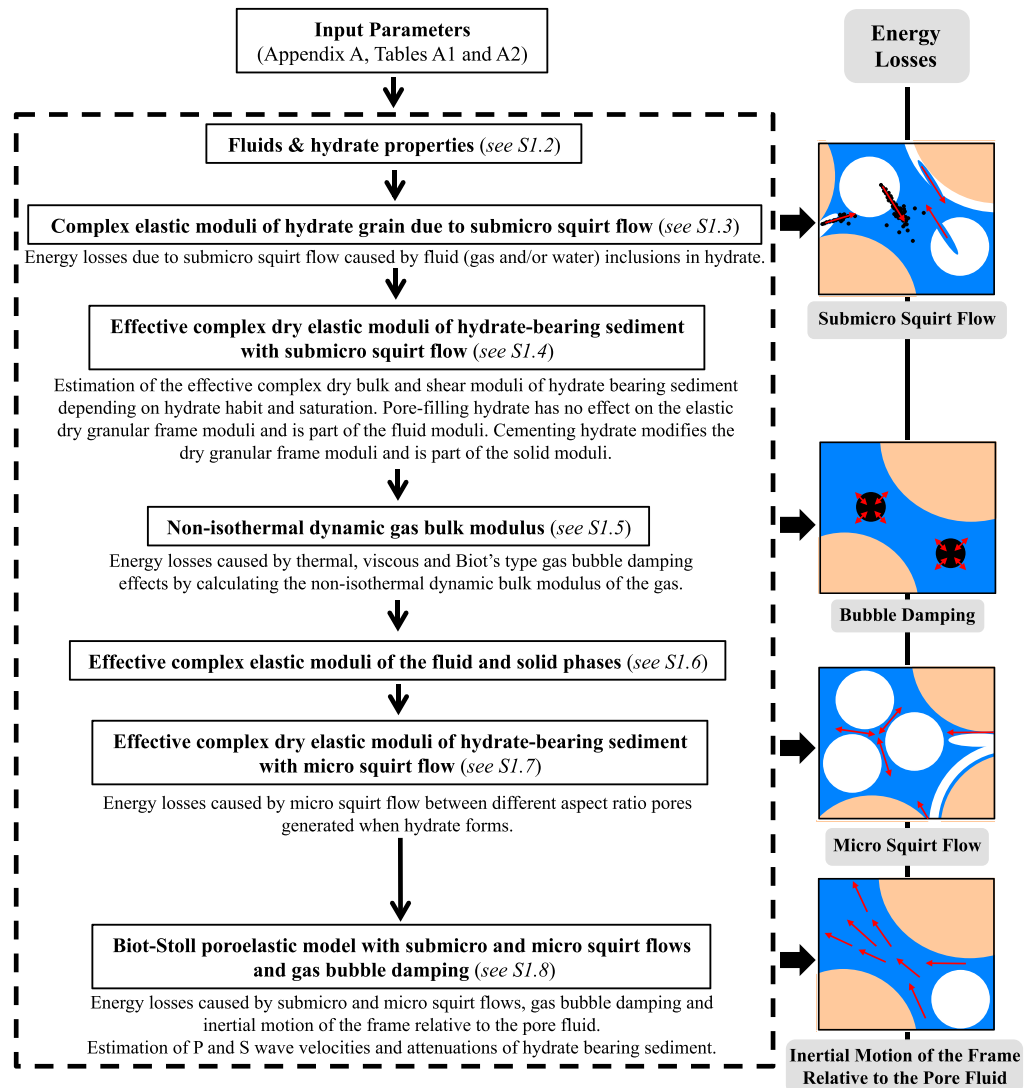


Figure 2. Workflow of the Hydrate-Bearing Effective Sediment (HBES) model. The idealized conceptual illustrations on the right show the different individual attenuation mechanisms (not to scale). The total energy loss in the sediment with hydrate is given by the contribution of each of the attenuation mechanisms. The text in italics at the end of each box indicates the section in the supporting information with the detailed description of each procedure and its mathematical formulation.

of attenuation mechanisms occurring in hydrate-bearing sands (Figure 2). Our method calculates frequency-dependent *P* and *S* wave velocity and attenuation and includes elastic wave energy losses caused by (i) squirt flow between fluid inclusions in hydrate and the pores, (ii) squirt flow between different aspect ratio pores, (iii) inertial motion of the frame with respect to the pore fluid (Biot's type attenuation), and (iv) gas bubble damping (Figure 2). Other energy loss mechanisms possibly acting in gas hydrate systems but not implemented in our model may include wave-induced fluid flow at the mesoscale [White, 1975] and wave-induced gas exsolution-dissolution [Tisato et al., 2015]. The HBES model also considers how different hydrate habits affect both velocity and attenuation and allows representing cases where methane gas coexists with hydrate under hydrate stability conditions [Milkov et al., 2004; Lee and Collett, 2006; Paganoni et al., 2016]. First, we validate our model with published experimental *P* and *S* wave velocities and attenuations of hydrate-bearing sediments, and then we illustrate the sensitivity of *P* and *S* wave velocities and attenuations to input parameters in sediments with pore-filling hydrate. We show that different hydrate-related attenuation mechanisms may act at different elastic wave frequency ranges.

2. The Hydrate-Bearing Effective Sediment Model

The Hydrate-Bearing Effective Sediment model calculates frequency-dependent P and S wave velocity and attenuation of hydrate-bearing sediments (Figure 2). Here we describe the main theoretical concepts in which the HBES model is based, but the detailed description and complete mathematical formulation is given in the supporting information.

Experiments on natural and synthetic hydrates show a microporous structure [Kuhs *et al.*, 2004; Zhao *et al.*, 2015], and hence hydrates can be understood as a compliant material, due to inclusions of water and/or gas, and with a behavior resembling that of clay minerals [Best and McCann, 1995; Leurer, 1997]. Moreover, elevated P and S wave attenuations have been detected on hydrate-bearing sands [Guerin and Goldberg, 2002; Matsushima, 2006; Priest *et al.*, 2006]. Based on the above experiments and ideas, Priest *et al.* [2006] hypothesized that these elevated attenuations could be explained by (i) local viscous fluid flow (squirt flow) between low aspect ratio pore layers of water, bound to mineral grain surfaces when cementing hydrate forms, and the pores, and (ii) viscous squirt flow between connected low aspect ratio micropores inside the hydrate grains and the sediment pores. Best *et al.* [2013] considered the attenuation due to the latter type of squirt flow in their hydrate effective grain model. They calculated the complex shear and bulk moduli of hydrate applying the formulation from Johnston *et al.* [1979] which was later adapted by Leurer [1997] and Leurer and Brown [2008] to represent squirt flow between the structural water of clay minerals one-side connected to water in the pores. Best *et al.* [2013] adopted this formulation for fluid inclusions in hydrate and substituted the clay mineral bulk and shear moduli for those of the hydrate; for simplicity, they assumed single aspect ratio fluid inclusions in hydrate completely filled with either methane or water. The new HBES model employs Best *et al.*'s [2013] model framework and introduces the following: (i) pressure-temperature dependent density, bulk compressibility, and viscosity of methane and water; (ii) the possible coexistence of one-side connected ellipsoidal water and gas inclusions in hydrate, in which each phase can occupy micropores with different aspect ratios; (iii) local viscous squirt flow between two-side connected ellipsoidal pores generated when hydrate forms (defined as type 2 pores in the formulation; see supporting information) and the initial pores, in which each hydrate habit can create a different aspect ratio pore; and (iv) wave-induced frequency-dependent oscillating gas bubbles in a dilute gas-liquid mixture considering viscous, thermal, and Biot's type damping [Smeulders and van Dongen, 1997].

To distinguish between the two local viscous squirt flows considered in the HBES model, here we use the term submicro squirt flow for that between fluid inclusions in hydrate and the pores and micro squirt flow for that between hydrate-generated pores and the initial (e.g., pores of sand grain framework host) pores. First, we calculate the complex bulk and shear moduli of the hydrate grain considering submicro squirt flow, similar to Best *et al.* [2013], and introduce these into Ecker *et al.*'s [1998, 2000] formulation to obtain the complex dry elastic moduli of cementing and pore-filling hydrate-bearing sediment. Second, we calculate the nonisothermal frequency-dependent complex bulk modulus of the gas to consider energy losses caused by gas bubble damping. Third, we calculate the effective complex moduli of the pore fluid and solid phases. As assumed by Ecker *et al.* [1998], pore-filling hydrate is treated as part of the pore fluid and does not modify the elastic moduli of the dry granular frame but modifies the pore fluid bulk modulus. Therefore, the effective bulk modulus of the pore fluid can be complex and frequency dependent because submicro squirt flow and gas bubble damping generate a hydrate and gas, respectively, complex frequency-dependent bulk modulus. The effective bulk and shear moduli of the solid phase can also be complex and frequency dependent due to submicro squirt flow in cementing hydrate. Fourth, we consider micro squirt flow by applying the formulation from Leurer [1997] and Leurer and Brown [2008] and (i) substitute the bulk and shear moduli of the clay mineral by the real parts of the effective complex dry frame moduli of hydrate-bearing sediment, (ii) use the real part of the effective complex bulk modulus of the pore fluid, and (iii) assume two-side connected and hydrate-generated ellipsoidal pores. We calculate the final effective complex dry elastic moduli of the hydrate-bearing sediment by assuming superposition of squirt flow mechanisms. This means that the imaginary parts of the effective complex dry frame moduli caused by submicro squirt flow are added to the imaginary parts caused by micro squirt flow. Finally, we introduce the final effective complex dry frame moduli and the effective complex bulk modulus of the pore fluid (water, gas, and pore-filling hydrate) and solid (sediment grains and cementing hydrate) phases into the Biot-Stoll poroelastic model [Biot, 1956a, 1956b; Stoll and Bryan, 1970] to calculate P and S wave velocity and attenuation.

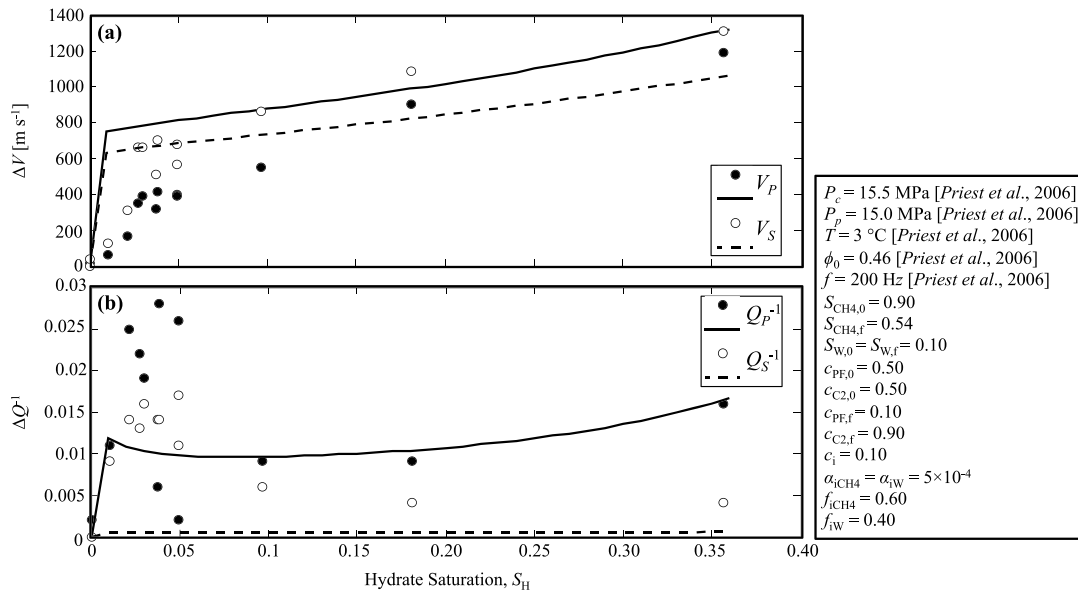


Figure 3. Comparison between measured values (dots) [Priest et al., 2006] and values calculated with the HBES model (lines) of P and S wave (a) water saturated velocity and (b) methane saturated attenuation, in sediment with hydrate relative to the values without hydrate. Modeled attenuation caused by submicro squirt flow and Biot’s type global fluid flow, but the relative contribution from the latter at 200 Hz is negligible. Measured results correspond to the excess gas method, and the P and S wave velocities were converted to water saturated samples using Gassmann’s equation [Priest et al., 2006]. The input parameters listed in the table and default input parameters are defined in Appendix A, Tables A1 and A2. The subscripts 0 and f in the table mean initial and final conditions.

3. HBES Model Performance: Results

3.1. Comparison With Experimental Data

We used the experimental measurements of P and S wave velocity (V_P , V_S) and attenuation (Q_P^{-1} , Q_S^{-1}) presented by Priest et al. [2006] to evaluate and validate the performance of the HBES model. Priest et al. [2006] formed hydrate under excess-gas conditions (methane saturated pore space) using a resonant-column apparatus and measured peaks in attenuation at hydrate saturations between 3% and 5% at seismic frequencies. They attributed these peaks to either squirt flow caused by monolayers of adsorbed water remaining at grain contacts when cementing hydrate forms (this mechanism belongs to our more general concept of micro squirt flow) or nanoporosity/inclusions of methane and/or water in hydrate (here named as submicro squirt flow). Our model captures the location of the peak in both Q_P^{-1} and Q_S^{-1} at hydrate saturations below 5% when considering (i) the presence of methane and water inclusions in hydrate and (ii) that a fraction of hydrate grows at grain contacts and the initial fraction of pore-filling hydrate in the model decreases linearly with hydrate saturation, and thus cementing hydrate in contact with the grains increases accordingly (Figure 3). In these experiments, at 3% to 5% hydrate saturation, sand grains are cemented by hydrate [Priest et al., 2005], consistent with our assumed hydrate habit distribution (see Figure 3, table). This habit distribution also captures the change in slope of P and S wave velocity observed at hydrate saturations below 5% and the magnitude of seismic velocity change with hydrate saturation (Figure 3a).

The model suggests that Q_P^{-1} is more sensitive to the presence of hydrate than Q_S^{-1} , as also measured experimentally. However, it gives smaller increments in attenuation than those measured, especially for Q_S^{-1} (Figure 3b). Lower changes in Q_S^{-1} than in Q_P^{-1} due to submicro squirt flow caused by intercrystalline water layers in clay minerals are also obtained by Leurer and Brown [2008]. Discrepancies between measured and modeled attenuations may be explained by (i) other possible attenuation mechanisms acting at seismic frequencies and not considered in our model, such as wave-induced fluid flow at the mesoscale [White, 1975] and/or wave-induced gas exsolution-dissolution [Tisato et al., 2015], and (ii) the idealized nature of our analytical effective approach, including the geometries considered and their distributions. More notable, the model is able to capture the trend in observed Q_P^{-1} and Q_S^{-1} changes with hydrate saturation in the range between 0% to 35% (Figure 3b). We also tested if the observed changes in V_P , V_S , Q_P^{-1} , and Q_S^{-1} could be caused by micro squirt flow only, but we were not able to obtain any sensible match to the data.

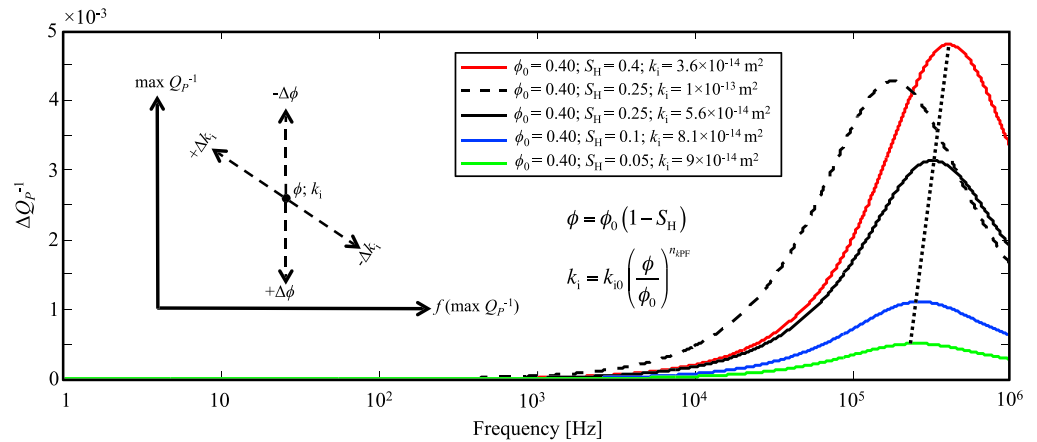


Figure 4. Variation in P wave attenuation with frequency in sediment with pore-filling hydrate relative to the values without hydrate. Results for partially water saturated pores ($S_W = 1 - S_H$). Attenuation caused by Biot’s type global fluid flow, without considering hydrate-related squirt flow mechanisms. The black dotted line joining the attenuation peaks shows the translation of the peaks toward higher frequencies with the reduction in intrinsic permeability. The inset shows a conceptual diagram of how changes in intrinsic permeability and porosity affect the maximum attenuation and the frequency at which the maximum attenuation occurs. Input parameters are defined in Appendix A, Tables A1 and A2.

Submicro squirt flow due to methane and water inclusions could partly explain the attenuation behavior observed in Priest *et al.* [2006] samples and, at seismic frequencies, may be the primary hydrate-related attenuation mechanism.

3.2. Elastic Behavior of Sediments With Pore-Filling Hydrate

Here we present model results for pore-filling hydrate-bearing sediments (see justification in sections 1 and 4) and for P wave velocity and attenuation only. Similar to Leurer and Brown’s [2008] results for submicro squirt flow caused by intercrystalline water layers in clay minerals, we found that frequency-related changes in S wave velocity and attenuation caused by pore-filling hydrate-generated squirt flow are smaller than those from P waves and are not discussed further here. To isolate intrinsic hydrate-related processes, we use the absolute difference between the P wave velocity and attenuation of the sediment with pore-filling hydrate and those from the host sediment only.

The sole presence of pore-filling hydrate in the sediment reduces the porosity and intrinsic permeability of the sediment, and these produce two opposite effects in the maximum P wave attenuation at high frequencies. If the available porosity reduces, the surface contact area between the fluid in the pores and the solids increases. This results in higher attenuation values caused by higher viscous drag between the solids and global fluid flow (Biot’s type attenuation mechanism) and a attenuation peak located at a frequency independent of pore-filling hydrate saturation. If the intrinsic permeability reduces, so does Biot’s type attenuation (less global fluid flow), and the attenuation peak moves to higher frequencies (see Figure 4, inset). The net effect on attenuation depends on the rate at which intrinsic permeability decreases with porosity, and so with pore-filling hydrate saturation, which in our formulation is controlled by the n_{kPF} parameter, here assumed to be 2 (Appendix A, Table A1, and Supporting Information Eq. S23). In Figure 4, the increase in attenuation caused by the reduction in porosity dominates over the decrease caused by the reduction in intrinsic permeability, and so the attenuation increases with pore-filling hydrate saturation.

From a phenomenological perspective, the Kramers-Kronig relations state that any change in attenuation needs to be related with a change in velocity dispersion [e.g., Mavko *et al.*, 2009]. That is, larger attenuations are necessarily linked with larger velocity dispersions, and zero attenuation requires zero velocity dispersion. Our HBES model predicts frequency-related changes in velocity at frequencies where attenuation changes also occur (Figure 5). In Figure 5b, attenuation peaks shown at seismic frequencies are caused by fluid inclusions in hydrate (submicro squirt flow) whereas at ultrasound frequencies they are caused by both the reduction in the available porosity due to pore-filling hydrate and the presence of different aspect ratio pores. Attenuation maxima due to submicro squirt flow generated by fluid inclusions in hydrate occur over the whole frequency range, depending on both the aspect ratio and type of fluid in the inclusions (Figures 6a and 6b), whereas peaks

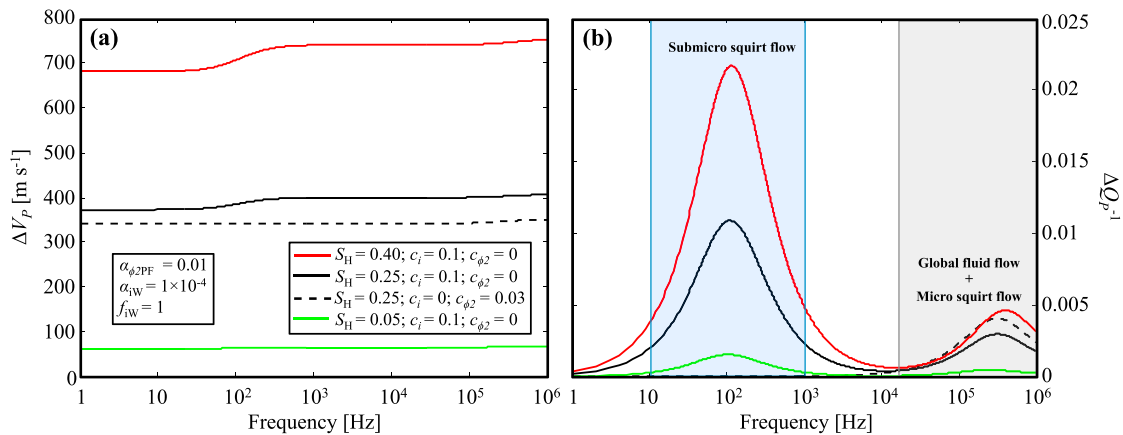


Figure 5. Variation in *P* wave (a) velocity and (b) attenuation with frequency in sediment with pore-filling hydrate relative to the values without hydrate. Results for partially water saturated pores ($S_W = 1 - S_H$). Attenuation caused by Biot’s type global fluid flow and submicro and micro squirt flows. Input parameters are defined in Appendix A, Tables A1 and A2.

due to micro squirt flow generated by different aspect ratio pores occur at sonic to ultrasound frequencies, independent of the aspect ratio of pores (Figure 6c). In our formulation, micro squirt flow is related with the composite’s dry effective moduli. This means that micro squirt flow contributes to the attenuation generated by the global fluid flow in the pore network and hence is more significant at high frequencies. This frequency distinction imposes further constraints on hydrate saturations that can reproduce broadband elastic measurements. For a given frequency, maximum changes in *P* wave velocity and attenuation are observed for a particular aspect ratio and type of fluid inclusion in hydrate (Figures 6a, 6b, 7a, and 7b). For a fixed aspect ratio, the magnitude of these changes depends on the fluid type and concentration of inclusions (Figures 6b, 7c, and 7d). Essentially, the type of fluid inclusion in hydrate controls both the magnitude of attenuation changes and the frequency at which the attenuation peak is located. In contrast, the aspect ratio of fluid inclusions in hydrate controls only the frequency dependence of the attenuation peak, and the concentration of inclusions controls only the magnitude of attenuation.

In the results described above, we have assumed that the sediment pores are only occupied by water and hydrate to better understand and isolate pore-filling hydrate-related changes in elastic wave attenuation. However, several gas hydrate fields have shown evidence of coexisting methane gas and hydrate in sediments within the gas hydrate stability zone [e.g., Lee and Collett, 2006]. The HBES model can also be used to study frequency-dependent changes in attenuation caused by gas bubbles in the pores. At low frequencies, the presence of methane gas bubbles in the pores reduces considerably the *P* wave velocity, whereas at high frequencies the *P* wave velocity is higher than that for the fully water saturated case (Figure 8a). At the high frequency limit, the *P* wave velocity tends exactly to that of the fully water saturated case, as stated by Smeulders and van Dongen [1997]. When hydrate is present in the pores, at low frequencies there is a smaller decrease in *P* wave velocity due to gas bubbles (Figure 8a, solid red and black lines). Two distinctive peaks in attenuation at ~5 Hz and between 10 and 30 kHz are obtained with a gas bubble radius of 0.001 m, and the latter attenuation peak moves to higher frequencies when decreasing the bubble radius (Figure 8b). The greater high frequency attenuation peak observed for a free methane gas saturation of 10% and pore-filling hydrate, in comparison to that without hydrate (Figure 8b, solid red and black lines), is caused by hydrate-driven reduction in porosity generating higher Biot’s type global fluid flow attenuation.

4. Discussion

There is general consensus in the literature on the physical mechanisms explaining the effects of different hydrate habits on *P* and *S* wave velocities. Pore-filling hydrate-bearing sediments do not show significant changes in *P* and *S* wave velocities with respect to the host sediment [Priest et al., 2009; Waite et al., 2009; Dai et al., 2012], because hydrate floats in the pore fluid and thus only increases the bulk modulus of the pore fluid [Ecker et al., 1998]. Load-bearing and cementing hydrate-bearing sediments show higher *P* and *S* wave velocities than those of the host sediment [Priest et al., 2009; Waite et al., 2009; Dai et al., 2012] because hydrate

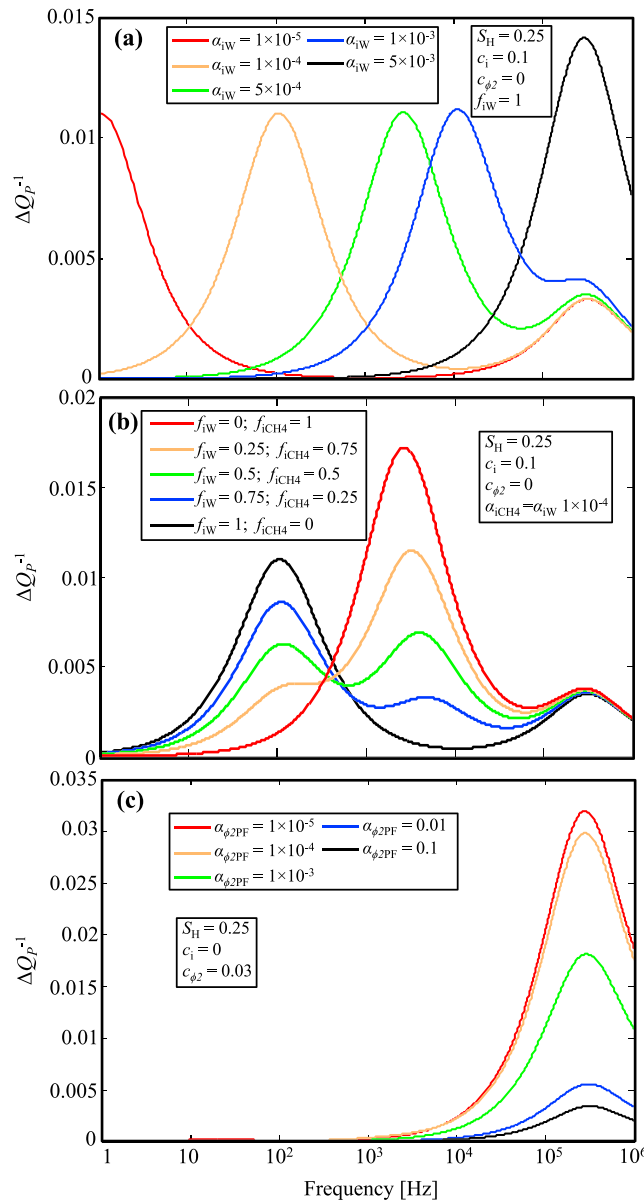


Figure 6. Variation in P wave attenuation with frequency in sediment with pore-filling hydrate relative to the values without hydrate. Results for partially water saturated pores ($S_W = 1 - S_H$) and for a hydrate saturation (S_H) of 0.25. (a and b) Attenuation caused by Biot's type global fluid flow and submicro squirt flow and (c) Biot's type global fluid flow and micro squirt flow. Input parameters are defined in Appendix A, Tables A1 and A2.

increases the composite's bulk and shear moduli [Ecker et al., 1998]. In contrast, the way in which different hydrate habits affect attenuation is an open scientific question. Some studies suggest that the presence of hydrate in the sediments reduces attenuation [Dvorkin et al., 2003; Westbrook et al., 2008; Dewangan et al., 2014], while others suggest it increases attenuation [Dvorkin and Uden, 2004; Guerin and Goldberg, 2002; Pratt et al., 2005; Matsushima, 2006; Priest et al., 2006; Sun et al., 2016]. Also, part of the enhanced attenuations measured in hydrate-bearing sediments may be due to a source-coupling effect [Lee, 2006]. When the hydrate grains are larger than the sediment grains, hydrate forms nodules or veins, and this can cause either a negligible effect on attenuation, such as in the Blake Ridge [Wood et al., 2000], or a reduction, such as offshore west of Svalbard [Westbrook et al., 2008] and in the KG Basin [Dewangan et al., 2014]. Our results are consistent with the experimental [e.g., Priest et al., 2006] and field studies where attenuation increased and hydrate was in pore-filling morphology within sand dominated sediments [e.g., Mallik well, Pratt et al., 2005].

Several studies have speculated [e.g., Milkov et al., 2004; Miyakawa et al., 2014; Goswami et al., 2015], proposed [Darnell and Flemings, 2015], and demonstrated experimentally [Sahoo et al., n.d., submitted] that gas can coexist with hydrate within the hydrate stability zone (HSZ). This gas can (i) fill inclusions in hydrate allowing local viscous flow between those

and the pores (submicro squirt flow), (ii) stay in the pores allowing local viscous flow due to different aspect ratio pores generated when hydrate grows (micro squirt flow), and (iii) stay in the pores allowing gas bubble damping effects. Priest et al. [2006] present a mechanism in which local viscous fluid flow occurs between monolayers of water remaining at grain contacts (when cementing hydrate forms) and the pores. This idea can be extended to the formation of pore-filling hydrate as, in principle, the formation of pore-filling hydrate can also generate micro squirt flow (Figure 2). However, the mechanism presented by Priest et al. [2006] is likely to produce higher attenuations, as the monolayers of adsorbed water are likely to have lower aspect ratios (Figure 6c). It is sensible to expect that both submicro and micro squirt flows can occur in sediments with hydrate independent of hydrate habit.

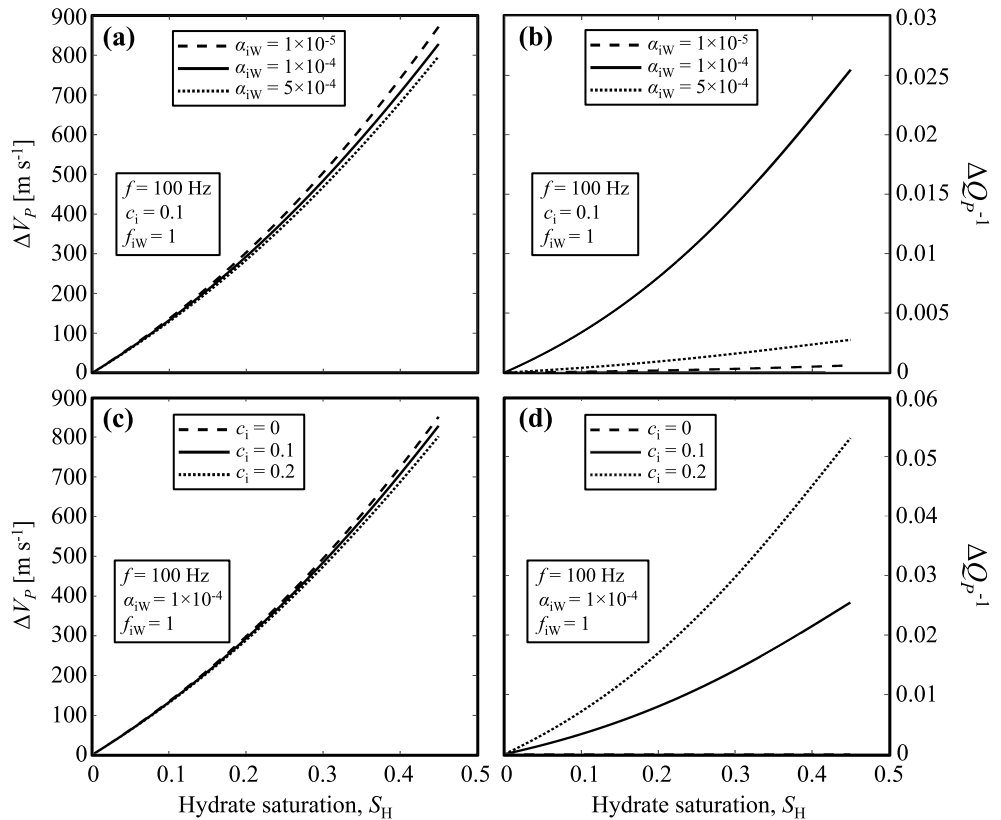


Figure 7. Variation in *P* wave (a and c) velocity and (b and c) attenuation with pore-filling hydrate saturation in sediment relative to the values without hydrate. Results are shown for partially water saturated pores ($S_W = 1 - S_H$) and fully water saturated inclusions in hydrate ($f_{iW} = 1$), and for a frequency (f) of 100 Hz. Attenuation caused by submicro squirt flow and Biot's type global fluid flow, but the relative contribution from the latter at 100 Hz is negligible. Input parameters are defined in Appendix A, Tables A1 and A2. Note that in Figure 7d the dashed line is not visible, is overlapping the x axis, because the concentration of fluid inclusions in hydrate (c_i) is zero and hence no variation in attenuation occurs due to submicro squirt flow.

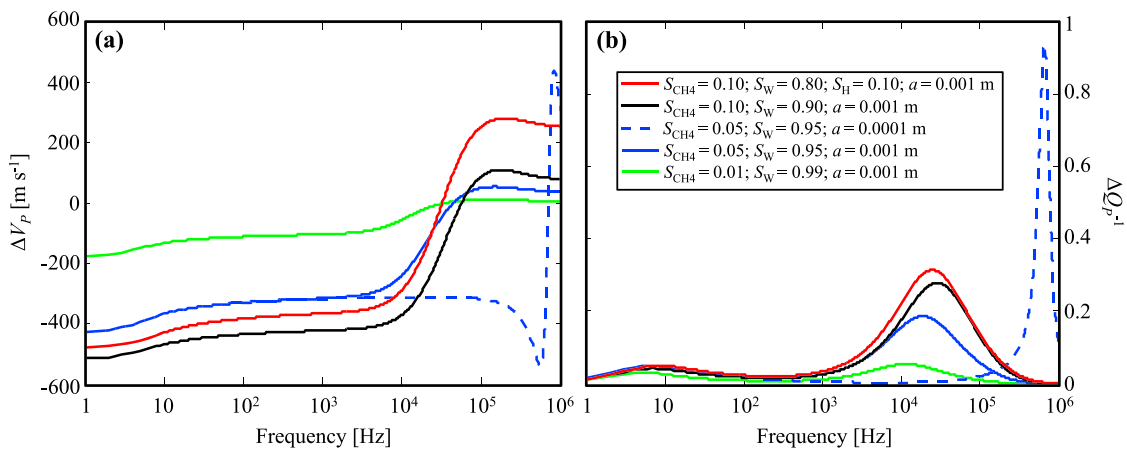


Figure 8. Variation in *P* wave (a) velocity and (b) attenuation with frequency in sediment with gas bubbles and pore-filling hydrate relative to the values with fully water saturated pores. Results for two methane bubble sizes (a of 0.001 m and 0.0001 m) and different combinations of water, free methane gas, and hydrate saturations. Attenuation caused by gas bubble damping and Biot's type global fluid flow. Hydrate-related squirt flow attenuation is not considered in the model run with pore-filling hydrate (red lines). Input parameters are defined in Appendix A, Tables A1 and A2.

The main drawback to the use of P and S wave attenuation as a parameter for estimating hydrate saturation is that, traditionally, attenuation models have treated wave velocity and attenuation independently [Lee, 2006] which potentially contravenes the Kramers-Kronig relations of causality [e.g., Mavko et al., 2009]. Our proposed HBES model is causal and includes several important hydrate systems-related features affecting P and S wave velocity and attenuation such as the following: derivation of fluid properties from equations of state, coexistence of gas and hydrate within the HSZ, submicro and micro squirt flows of gas and/or water, gas bubble damping, possible coexistence of different hydrate habits, and the ability to alter global fluid flow energy losses due to porosity and intrinsic permeability changes. The HBES model adds valuable insights to those already learned from the limited number of published causal attenuation models [e.g., Guerin and Goldberg, 2005; Best et al., 2013].

5. Conclusions

The sole presence of pore-filling hydrate affects both the porosity and intrinsic permeability of the sediment, and hence the attenuation caused by the inertial motion of the grains with respect to the fluid in the pores at high frequencies above 10^4 Hz. Moreover, local submicro and micro squirt flows can also explain enhanced attenuations in pore-filling hydrate-bearing sediments at frequencies from 1 to 10^6 Hz that span the entire frequency range of interest to exploration seismology. In methane-rich systems within the HSZ, the absence of a distinctive increase in seismic wave velocity from that expected of the host sediment only suggests that cementing or load-bearing hydrates are unlikely to be present in the system. However, this does not exclude the possible presence of pore-filling hydrate. From a conventional seismic exploration point of view, enhanced attenuation caused by fluid inclusions in hydrate may be the only hydrate-related loss mechanism able to produce the seismic signal contrasts needed to detect whether a reservoir sand is likely to have pore-filling hydrate, or not. If no distinctive peak in attenuation is observed, this can also mean that pore-filling hydrate still exists but it does not contain sufficient and/or adequate inclusions to create a detectable change in attenuation at seismic frequencies. Overall, our results provide a physical basis for interpreting seismic attenuation observations in sediments with pore-filling methane hydrate.

Appendix A: Input Parameters

Table A1. Fixed Input Parameters Used in the Model Runs (Except in Figure 3; for More Detail, Refer to the Supporting Information)

Parameter	Symbol	Value	Unit	Reference
Test conditions ^a				
Confining pressure	P_c	2.5×10^7	Pa	
Pore fluid pressure	P_p	2.0×10^7	Pa	
Temperature	T	13	°C	
Components properties				
Hydrate bulk modulus	K_H	7.9×10^9	Pa	[Best et al., 2013]
Hydrate shear modulus	G_H	3.3×10^9	Pa	[Best et al., 2013]
Hydrate Poisson's ratio	ν_H	0.32		
Hydrate density	ρ_H	925	kg m^{-3}	[Helgerud et al., 2009]
Methane bulk modulus	K_{CH_4}	$K_{CH_4}(P_p, T)$	Pa	[Millero et al., 1980]
Methane density	ρ_{CH_4}	$\rho_{CH_4}(P_p, T)$	kg m^{-3}	[Millero et al., 1980]
Methane viscosity	μ_{CH_4}	$\mu_{CH_4}(P_p, T)$	Pa s	[Millero et al., 1980]
Methane irreducible saturation	S_{rCH_4}	0.02		[Reagan and Moridis, 2008]
Sand/quartz grain bulk modulus	K_S	36×10^9	Pa	[Ecker et al., 2000]
Sand/quartz grain shear modulus	G_S	45×10^9	Pa	[Ecker et al., 2000]
Sand/quartz grain Poisson's ratio	ν_S	0.062		
Sand/quartz grain density	ρ_S	2650	kg m^{-3}	[Ecker et al., 2000]
Sand/quartz grain diameter	d_S	1×10^{-4}	m	[Best et al., 2013]
Sand/quartz grain coordination number	n	8.5		[Ecker et al., 2000]
Water bulk modulus	K_W	$K_W(P_p, T)$	Pa	[Setzmann and Wagner, 1991]
Water density	ρ_W	$\rho_W(P_p, T)$	kg m^{-3}	[Setzmann and Wagner, 1991]
Water viscosity	μ_W	$\mu_W(P_p, T)$	Pa s	[Setzmann and Wagner, 1991]
Water salinity	s	3.5	% wt	
Water irreducible saturation	S_{rW}	0.2		[Reagan and Moridis, 2008]

Table A1. (continued)

Parameter	Symbol	Value	Unit	Reference
Sand sediment properties				
Porosity ^a without hydrate	φ_0	0.40		[Daigle et al., 2015]
Critical porosity	φ_c	0.38		[Best et al., 2013]
Intrinsic permeability without hydrate	k_0	10^{-13}	m ²	[Daigle et al., 2015]
Intrinsic permeability exponent for cementing hydrate	n_{kC}	3		
Intrinsic permeability exponent for pore-filling hydrate	n_{kPF}	2		
Tortuosity	t	3		based on [Mavko et al., 2009]
van Genuchten's [1980] capillary pressure fitting parameter	m	0.45		[Reagan and Moridis, 2008]
van Genuchten's [1980] capillary pressure gas entry parameter	P_0	2000	Pa	[Reagan and Moridis, 2008]

^aTest conditions and porosity represent those of a hydrate-bearing sand at about 1500 m water depth and 500 m below the seabed. We have considered the geothermal structure in the northern Gulf of Mexico with a seabed temperature of 4°C and a geothermal gradient of 17.9°C km⁻¹ [Daigle et al., 2015].

Table A2. Case-Dependent Input parameters Used in the Model Runs (for More Detail, Refer to the Supporting Information)

Parameter	Symbol	Unit
Aspect ratio of inclusions containing methane or water	$\alpha_{\{CH_4, IW\}}$	
Aspect ratio of type 2 pores created by the formation of cementing hydrate enveloping the grains (C1) and in contact with the grains (C2), and pore-filling hydrate (PF)	$\alpha_{\varphi 2\{C1, C2, PF\}}$	
Methane bubble radius	a	m
Concentration of cementing hydrate enveloping the grains (C1) and in contact with the grains (C2), and pore-filling hydrate (PF)	$c_{\{C1, C2, PF\}}$	
Concentration of inclusions in hydrate	c_i	
Concentration of different aspect ratio, type 2 pores	$c_{\varphi 2}$	
Frequency	f	Hz
Fraction of cementing hydrate enveloping the grains	f_{C1}	
Fraction of methane and water inclusions in hydrate	$f_{\{CH_4, IW\}}$	
Intrinsic permeability	k	m ²
Porosity	φ	
Saturation of hydrate, methane, and water in the pore space	$S_{\{H, CH_4, W\}}$	

Acknowledgments

We acknowledge funding from the United Kingdom Natural Environment Research Council (NE/J020753/1). The data used are listed in the references, tables, figures, and in an Excel spreadsheet in the supporting information. The references Berryman [1995]; Bishop [1959]; Dvorkin et al. [1999]; Hovem and Ingram [1979]; Ishii and Mishima [1984]; Kuster and Toksöz [1974]; Mahabadi et al. [2016]; Mindlin [1949], and Reuss [1929] refer only to the supporting information. We thank Nicola Tisato and an anonymous reviewer for their detailed and constructive comments.

References

- Berryman, J. G. (1995), Mixture theories for rock properties, in *Rock Physics and Phase Relations: A Handbook of Physical Constants*, edited by T. J. Ahrens, pp. 205–228, AGU, Washington, D. C.
- Best, A. I., and C. McCann (1995), Seismic attenuation and pore-fluid viscosity in clay-rich reservoir sandstones, *Geophysics*, *60*(5), 1386–1397, doi:10.1190/1.1443874.
- Best, A. I., J. A. Priest, C. R. I. Clayton, and E. V. L. Rees (2013), The effect of methane hydrate morphology and water saturation on seismic wave attenuation in sand under shallow sub-seafloor conditions, *Earth Planet. Sci. Lett.*, *368*, 78–87, doi:10.1016/j.epsl.2013.02.033.
- Biot, M. A. (1956a), Theory of propagation of elastic waves in a fluid-saturated porous solid. I. Low-frequency range, *J. Acoust. Soc. Am.*, *28*(2), 168–178, doi:10.1121/1.1908239.
- Biot, M. A. (1956b), Theory of propagation of elastic waves in a fluid-saturated porous solid. II. Higher frequency range, *J. Acoust. Soc. Am.*, *28*(2), 179–191, doi:10.1121/1.1908241.
- Bishop, A. W. (1959), The principle of effective stress, *Tek. Ukebl.*, *106*(39), 859–863.
- Boswell, R., and T. S. Collett (2011), Current perspectives on gas hydrate resources, *Energy Environ. Sci.*, *4*(4), 1206–1215, doi:10.1039/C0EE00203H.
- Boswell, R., D. Shelander, M. Lee, T. Latham, T. Collett, G. Guerin, G. Moridis, M. Reagan, and D. Goldberg (2009), Occurrence of gas hydrate in Oligocene Frio sand: Alaminos Canyon Block 818: Northern Gulf of Mexico, *Mar. Pet. Geol.*, *26*(8), 1499–1512, doi:10.1016/j.marpetgeo.2009.03.005.
- Chand, S., T. A. Minshull, J. A. Priest, A. I. Best, C. R. I. Clayton, and W. F. Waite (2006), An effective medium inversion algorithm for gas hydrate quantification and its application to laboratory and borehole measurements of gas hydrate-bearing sediments, *Geophys. J. Int.*, *166*(2), 543–552, doi:10.1111/j.1365-246X.2006.03038.x.
- Choi, J.-H., S. Dai, J.-H. Cha, and Y. Seol (2014), Laboratory formation of noncementing hydrates in sandy sediments, *Geochem. Geophys. Geosyst.*, *15*, 1648–1656, doi:10.1002/2014GC005287.
- Dai, S., J. C. Santamarina, W. F. Waite, and T. J. Kneafsey (2012), Hydrate morphology: Physical properties of sands with patchy hydrate saturation, *J. Geophys. Res.*, *117*, B11205, doi:10.1029/2012JB009667.

- Daigle, H., A. Cook, and A. Malinverno (2015), Permeability and porosity of hydrate-bearing sediments in the northern Gulf of Mexico, *Mar. Pet. Geol.*, *68*(Part A), 551–564, doi:10.1016/j.marpetgeo.2015.10.004.
- Darnell, K. N., and P. B. Flemings (2015), Transient seafloor venting on continental slopes from warming-induced methane hydrate dissociation, *Geophys. Res. Lett.*, *42*, 10,765–10,772, doi:10.1002/2015GL067012.
- Dewangan, P., R. Mandal, P. Jaiswal, T. Ramprasad, and G. Sriram (2014), Estimation of seismic attenuation of gas hydrate bearing sediments from multi-channel seismic data: A case study from Krishna–Godavari offshore basin, *Mar. Pet. Geol.*, *58*(Part A), 356–367, doi:10.1016/j.marpetgeo.2014.05.015.
- Dvorkin, J., and R. Uden (2004), Interpreter's corner—Seismic wave attenuation in a methane hydrate reservoir, *Leading Edge*, *23*, 730–732.
- Dvorkin, J., M. Prasad, A. Sakai, and D. Lavoie (1999), Elasticity of marine sediments: Rock physics modeling, *Geophys. Res. Lett.*, *26*(12), 1781–1784, doi:10.1029/1999GL900332.
- Dvorkin, J., A. Nur, R. Uden, and T. Taner (2003), Round table—Rock physics of a gas hydrate reservoir, *Leading Edge*, *22*, 842–847.
- Ecker, C., J. Dvorkin, and A. Nur (1998), Sediments with gas hydrates: Internal structure from seismic AVO, *Geophysics*, *63*(5), 1659–1669, doi:10.1190/1.1444462.
- Ecker, C., J. Dvorkin, and A. M. Nur (2000), Estimating the amount of gas hydrate and free gas from marine seismic data, *Geophysics*, *65*(2), 565–573, doi:10.1190/1.1444752.
- Goswami, B. K., K. A. Weitemeyer, T. A. Minshull, M. C. Sinha, G. K. Westbrook, A. Chabert, T. J. Henstock, and S. Ker (2015), A joint electromagnetic and seismic study of an active pockmark within the hydrate stability field at the Vestnesa Ridge, West Svalbard margin, *J. Geophys. Res. Solid Earth*, *120*, 6797–6822, doi:10.1002/2015JB012344.
- Guerin, G., and D. Goldberg (2002), Sonic waveform attenuation in gas hydrate-bearing sediments from the Mallik 2L-38 research well, Mackenzie Delta, Canada, *J. Geophys. Res.*, *107*(B5), 2088, doi:10.1029/2001JB000556.
- Guerin, G., and D. Goldberg (2005), Modeling of acoustic wave dissipation in gas hydrate-bearing sediments, *Geochem. Geophys. Geosyst.*, *6*, Q07010, doi:10.1029/2005GC000918.
- Helgerud, M. B., W. F. Waite, S. H. Kirby, and A. Nur (2009), Elastic wave speeds and moduli in polycrystalline ice Ih, sl methane hydrate, and sll methane-ethane hydrate, *J. Geophys. Res.*, *114*, B02212, doi:10.1029/2008JB006132.
- Hovem, J. M., and G. D. Ingram (1979), Viscous attenuation of sound in saturated sand, *J. Acoust. Soc. Am.*, *66*(6), 1807–1812, doi:10.1121/1.383653.
- Huang, J.-W., G. Bellefleur, and B. Milkereit (2009), Seismic modeling of multidimensional heterogeneity scales of Mallik gas hydrate reservoirs, Northwest Territories of Canada, *J. Geophys. Res.*, *114*, B07306, doi:10.1029/2008JB006172.
- Hyodo, M., J. Yoneda, N. Yoshimoto, and Y. Nakata (2013), Mechanical and dissociation properties of methane hydrate-bearing sand in deep seabed, *Soils Found.*, *53*(2), 299–314, doi:10.1016/j.sandf.2013.02.010.
- Ishii, M., and K. Mishima (1984), Two-fluid model and hydrodynamic constitutive relations, *Nucl. Eng. Des.*, *82*(2), 107–126, doi:10.1016/0029-5493(84)90207-3.
- Johnston, D. H., M. N. Toksöz, and A. Timur (1979), Attenuation of seismic waves in dry and saturated rocks: II. Mechanisms, *Geophysics*, *44*(4), 691–711, doi:10.1190/1.1440970.
- Konno, Y., Y. Jin, J. Yoneda, M. Kida, K. Egawa, T. Ito, K. Suzuki, and J. Nagao (2015), Effect of methane hydrate morphology on compressional wave velocity of sandy sediments: Analysis of pressure cores obtained in the Eastern Nankai Trough, *Mar. Pet. Geol.*, *66*(Part 2), 425–433, doi:10.1016/j.marpetgeo.2015.02.021.
- Kuhs, W. F., G. Genov, E. Goreschnik, A. Zeller, K. S. Techmer, and G. Bohrmann (2004), The impact of porous microstructures of gas hydrates on their macroscopic properties, *Int. J. Offshore Polar Eng.*, *14*(4).
- Kuster, G. T., and M. N. Toksöz (1974), Velocity and attenuation of seismic waves in two-phase media: Part 1. Theoretical formulations, *Geophysics*, *39*(5), 587–606, doi:10.1190/1.1440450.
- Lee, J. Y., J. W. Jung, M. H. Lee, J. J. Bahk, J. Choi, B. J. Ryu, and P. Schultheiss (2013), Pressure core based study of gas hydrates in the Ulleung Basin and implication for geomechanical controls on gas hydrate occurrence, *Mar. Pet. Geol.*, *47*, 85–98, doi:10.1016/j.marpetgeo.2013.05.021.
- Lee, M. W. (2002), Biot-Gassmann theory for velocities of gas hydrate-bearing sediments, *Geophysics*, *67*(6), 1711–1719, doi:10.1190/1.1527072.
- Lee, M. W. (2006), Is amplitude loss of sonic waveforms due to intrinsic attenuation or source coupling to the medium?, *Sci. Invest. Rep.* 2006-5120, 13 pp., U.S. Geol. Surv., Reston, Va.
- Lee, M. W., and T. S. Collett (2006), Gas hydrate and free gas saturations estimated from velocity logs on Hydrate Ridge, offshore Oregon, USA, in *Proc. Ocean Drill. Program Sci. Results*, vol. 204, edited by A. M. Tréhu et al., pp. 1–25. [Available at http://www.odp.tamu.edu/publications/204_SR/VOLUME/CHAPTERS/103.PDF.]
- Leurer, K. C. (1997), Attenuation in fine-grained marine sediments; extension of the Biot-Stoll model by the "effective grain model" (EGM), *Geophysics*, *62*(5), 1465–1479, doi:10.1190/1.1444250.
- Leurer, K. C., and C. Brown (2008), Acoustics of marine sediment under compaction: Binary grain-size model and viscoelastic extension of Biot's theory, *J. Acoust. Soc. Am.*, *123*(4), 1941–1951, doi:10.1121/1.2871839.
- Mahabadi, N., S. Dai, Y. Seol, T. Sup Yun, and J. Jang (2016), The water retention curve and relative permeability for gas production from hydrate-bearing sediments: Pore-network model simulation, *Geochem. Geophys. Geosyst.*, *17*, 3099–3110, doi:10.1002/2016GC006372.
- Matsumura, J. (2006), Seismic wave attenuation in methane hydrate-bearing sediments: Vertical seismic profiling data from the Nankai Trough exploratory well, offshore Tokai, central Japan, *J. Geophys. Res.*, *111*, B10101, doi:10.1029/2005JB004031.
- Mavko, G., T. Mukerji, and J. Dvorkin (2009), *The Rock Physics Handbook*, 2nd ed., Cambridge Univ. Press, New York.
- Milkov, A. V., G. R. Dickens, G. E. Claypool, Y.-J. Lee, W. S. Borowski, M. E. Torres, W. Xu, H. Tomaru, A. M. Tréhu, and P. Schultheiss (2004), Coexistence of gas hydrate, free gas, and brine within the regional gas hydrate stability zone at Hydrate Ridge (Oregon margin): Evidence from prolonged degassing of a pressurized core, *Earth Planet. Sci. Lett.*, *222*(3–4), 829–843, doi:10.1016/j.epsl.2004.03.028.
- Millero, F. J., C.-T. Chen, A. Bradshaw, and K. Schleicher (1980), A new high pressure equation of state for seawater, *Deep Sea Res., Part A*, *27*(3), 255–264, doi:10.1016/0198-0149(80)90016-3.
- Mindlin, R. D. (1949), Compliance of elastic bodies in contact, *Trans. ASME*, *71*, A-259, doi:10.1007/978-1-4613-8865-4_24.
- Miyakawa, A., S. Saito, Y. Yamada, H. Tomaru, M. Kinoshita, and T. Tsuji (2014), Gas hydrate saturation at Site C0002, IODP Expeditions 314 and 315, in the Kumano Basin, Nankai trough, *Island Arc*, *23*(2), 142–156, doi:10.1111/iar.12064.
- Paganoni, M., J. A. Cartwright, M. Foschi, R. C. Shipp, and P. Van Rensbergen (2016), Structure II gas hydrates found below the bottom-simulating reflector, *Geophys. Res. Lett.*, *43*, 5696–5706, doi:10.1002/2016GL069452.
- Pratt, R. G., F. Hou, K. Bauer, and M. Weber (2005), Waveform tomography images of velocity and inelastic attenuation from the Mallik 2002 cross-hole seismic surveys, in *Scientific Results from the Mallik 2002 Gas Hydrate Production Research Well Program, Mackenzie Delta, Northwest Territories, Canada*, *Bull. Geol. Sur. Can.*, vol. 585, edited by S. R. Dallimore and T. S. Collett, pp. 14.

- Priest, J. A., A. I. Best, and C. R. I. Clayton (2005), A laboratory investigation into the seismic velocities of methane gas hydrate-bearing sand, *J. Geophys. Res.*, *110*, B04102, doi:10.1029/2004JB003259.
- Priest, J. A., A. I. Best, and C. R. I. Clayton (2006), Attenuation of seismic waves in methane gas hydrate-bearing sand, *Geophys. J. Int.*, *164*(1), 149–159, doi:10.1111/j.1365-246X.2005.02831.x.
- Priest, J. A., E. V. L. Rees, and C. R. I. Clayton (2009), Influence of gas hydrate morphology on the seismic velocities of sands, *J. Geophys. Res.*, *114*, B11205, doi:10.1029/2009JB006284.
- Priest, J. A., M. Druce, J. Roberts, P. Schultheiss, Y. Nakatsuka, and K. Suzuki (2015), PCATS Triaxial: A new geotechnical apparatus for characterizing pressure cores from the Nankai Trough, Japan, *Mar. Pet. Geol.*, *66*(Part 2), 460–470, doi:10.1016/j.marpetgeo.2014.12.005.
- Reagan, M. T., and G. J. Moridis (2008), Dynamic response of oceanic hydrate deposits to ocean temperature change, *J. Geophys. Res.*, *113*, C12023, doi:10.1029/2008JC004938.
- Reuss, A. (1929), Berechnung der Fließgrenzen von Mischkristallen auf Grund der Plastizitätsbedingung für Einkristalle, *J. Appl. Math. Mech.*, *9*, 49–58.
- Sahoo, S., H. Marín-Moreno, L. J. North, A. I. Best, and T. A. Minshull (n.d., submitted to *Geophysical Journal International*), Presence and consequences of co-existing gas and hydrate in the hydrate stability zone.
- Santamarina, J. C., et al. (2015), Hydro-bio-geomechanical properties of hydrate-bearing sediments from Nankai Trough, *Mar. Pet. Geol.*, *66*(Part 2), 434–450, doi:10.1016/j.marpetgeo.2015.02.033.
- Setzmann, U., and W. Wagner (1991), A new equation of state and tables of thermodynamic properties for methane covering the range from the melting line to 625 K at pressures up to 100 MPa, *J. Phys. Chem. Ref. Data*, *20*(6), 1061–1155, doi:10.1063/1.555898.
- Smeulders, D. M. J., and M. E. H. van Dongen (1997), Wave propagation in porous media containing a dilute gas–liquid mixture: Theory and experiments, *J. Fluid Mech.*, *1343*, 351–373, doi:10.1017/S0022112097005983.
- Spangenberg, E. (2001), Modeling of the influence of gas hydrate content on the electrical properties of porous sediments, *J. Geophys. Res.*, *106*(B4), 6535–6548, doi:10.1029/2000JB900434.
- Spangenberg, E., and J. Kulenkampff (2006), Influence of methane hydrate content on electrical sediment properties, *Geophys. Res. Lett.*, *33*, L24315, doi:10.1029/2006GL028188.
- Stern, L. A., T. D. Lorenson, and J. C. Pinkston (2011), Gas hydrate characterization and grain-scale imaging of recovered cores from the Mount Elbert Gas Hydrate Stratigraphic Test Well, Alaska North Slope, *Mar. Pet. Geol.*, *28*(2), 394–403, doi:10.1016/j.marpetgeo.2009.08.003.
- Stoll, R. D., and G. M. Bryan (1970), Wave attenuation in saturated sediments, *J. Acoust. Soc. Am.*, *47*(5B), 1440–1447, doi:10.1121/1.1912054.
- Sun, L. F., B. Milkereit, and N. Tisato (2016), Analysis of velocity dispersion using full-waveform multichannel sonic logging data: A case study, *Geophys. Prospect.*, *64*(4), 1016–1029, doi:10.1111/1365-2478.12410.
- Tamaki, K., et al. (1990), *Proceedings of the Ocean Drilling Program, Initial Reports*, 127, Ocean Drilling Program, College Station, Texas, doi:10.2973/odp.proc.ir.127.1990.
- Tisato, N., B. Quintal, S. Chapman, Y. Podladchikov, and J.-P. Burg (2015), Bubbles attenuate elastic waves at seismic frequencies: First experimental evidence, *Geophys. Res. Lett.*, *42*, 3880–3887, doi:10.1002/2015GL063538.
- Uchida, T., S. Dallimore, and J. U. N. Mikami (2000), Occurrences of natural gas hydrates beneath the permafrost zone in Mackenzie Delta: Visual and X-ray CT imagery, *Ann. N.Y. Acad. Sci.*, *912*(1), 1021–1033, doi:10.1111/j.1749-6632.2000.tb06857.x.
- van Genuchten, M. T. (1980), A closed-form equation for predicting the hydraulic conductivity of unsaturated soils, *Soil Sci. Soc. Am. J.*, *44*(5), 892–898, doi:10.2136/sssaj1980.03615995004400050002x.
- Waite, W. F., et al. (2009), Physical properties of hydrate-bearing sediments, *Rev. Geophys.*, *47*, RG4003, doi:10.1029/2008RG000279.
- Weitemeyer, K. A., S. C. Constable, K. W. Key, and J. P. Behrens (2006), First results from a marine controlled-source electromagnetic survey to detect gas hydrates offshore Oregon, *Geophys. Res. Lett.*, *33*, L03304, doi:10.1029/2005GL024896.
- Westbrook, G., S. Chand, G. Rossi, C. Long, S. Bünz, A. Camerlenghi, J. Carcione, S. Dean, J.-P. Foucher, and E. Flueh (2008), Estimation of gas hydrate concentration from multi-component seismic data at sites on the continental margins of NW Svalbard and the Storegga region of Norway, *Mar. Pet. Geol.*, *25*(8), 744–758, doi:10.1016/j.marpetgeo.2008.02.003.
- White, J. E. (1975), Computed seismic speeds and attenuation in rocks with partial gas saturation, *Geophysics*, *40*(2), 224–232, doi:10.1190/1.1440520.
- Winters, W., M. Walker, R. Hunter, T. Collett, R. Boswell, K. Rose, W. Waite, M. Torres, S. Patil, and A. Dandekar (2011), Physical properties of sediment from the Mount Elbert Gas Hydrate Stratigraphic Test Well, Alaska North Slope, *Mar. Pet. Geol.*, *28*(2), 361–380, doi:10.1016/j.marpetgeo.2010.01.008.
- Wood, W. T., W. S. Holbrook, and H. Hoskins (2000), In situ measurements of P wave attenuation in the methane hydrate and gas-bearing sediments of the Blake Ridge, in *Proceedings of the Ocean Drilling Program, Scientific Results*, vol. 164, edited by C. K. Paull et al., pp. 265–272.
- Yun, T. S., F. M. Francisca, J. C. Santamarina, and C. Ruppel (2005), Compressional and shear wave velocities in uncemented sediment containing gas hydrate, *Geophys. Res. Lett.*, *32*, L10609, doi:10.1029/2005GL022607.
- Zhao, J., L. Yang, Y. Liu, and Y. Song (2015), Microstructural characteristics of natural gas hydrates hosted in various sand sediments, *Phys. Chem. Chem. Phys.*, *17*(35), 22,632–22,641, doi:10.1039/C5CP03698D.